A Waveguide Model for UHF Propagation in Streets

Dana Porrat and Donald C. Cox
dporrat@wireless.stanford.edu, dcox@nova.stanford.edu
Stanford University, Stanford, CA 94305-9515, USA

Abstract

Radio frequency radiation in urban areas, emanating from a source lower than the surrounding buildings, propagates along streets. Urban streets with tall buildings on both sides are modeled as hollow slab waveguides made of lossy plates. The facade of the buildings is taken into account by introducing roughness onto the waveguide walls, which causes mode coupling in the waveguide. The electrical and geometrical properties of the waveguide walls induce a steady state distribution of power among the modes, which is attained at sufficient distances from the source.
Street junctions with line of sight to the source cause power to flow from the street containing the source around a corner and into a side street. The junction excites a distribution of power among the waveguide modes in the side street. As radiation flows along the side street, power is redistributed and eventually reaches a steady state. This propagation mechanism causes a significant decrease in power levels along the side street.
The predictions of average power levels received along side streets show satisfactory agreement with measurements taken in two urban environments.

1 Introduction

Measurements of received power in an urban environment show that street corners have a significant effect on the propagation of electromagnetic radiation in the UHF (300 MHz – 3 GHz) band. When measuring received power levels in urban paths, a strong decrease is evident when turning from a street with line of sight to the transmitter into a side street with no line of sight. This behavior of measured power levels has been modeled empirically: *Erceg et al.* [9] based their approach on optical ray theory and *Barbiroli et al.* [2] match mathematical forms to the measured shape of received power along the side street. Many authors mention an explanation based on the mode theory for wave propagation [3, 8, 15], and in this paper we develop this approach more rigorously.

Our model is based on the geometry of intersecting streets with very tall buildings on both sides. We assume that power flows along one street (the 'main' street) and couples into the other ('side') street. Each street is modeled as a waveguide made of infinitely large parallel plates with air in the middle. The waveguide is made of uniform lossy material where the electrical properties are representative of building materials. We consider the effect of the rough (non smooth) geometry of the walls by following the theory of *Marcuse* [23].

The model is presented in detail in section 2 and the theoretical predictions are compared to actual measurements in section 3.

2 The Model

A waveguide model with smooth walls is discussed in section 2.1 as a basis to the theory. This model is extended by considering rough (non-smooth) walls in section 2.2, the theory is based on optical fiber literature, in particular the publications of *Marcuse* [23]. The model of a street corner is presented in section 2.3.

2.1 A Smooth Multi-Moded Waveguide

The simple model we present here consists of a slab waveguide, which represents a street with very tall buildings on both sides. The walls of the

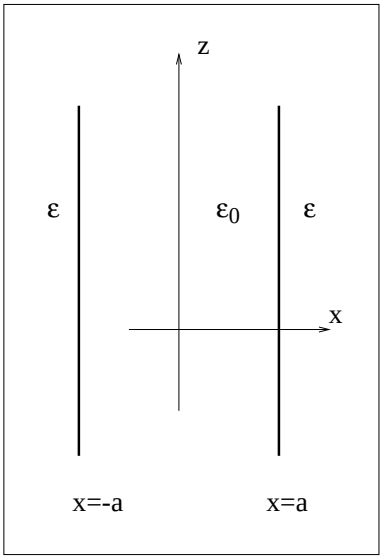

Figure 1: A smooth slab waveguide

waveguide are made of a smooth lossy dielectric material (figure 1). The waveguide is empty, so between the walls we assume the electrical properties of free space. With this simple model, we ignore the effects of the ground and any objects within the waveguide (such as people, cars and trees); these complications will be addressed at a later stage of our research. In this section we discuss a waveguide with smooth homogeneous walls, as a basis for the presentation of the more complicated waveguide with rough walls in the next section. The waveguide can be defined in terms of the relative complex dielectric constant of the walls ϵ:

$$\epsilon_s(x,z) = \begin{cases} 1 & |x| \leq a \\ \epsilon & |x| > a \end{cases} \qquad (1)$$

where $\epsilon_s(x,z)$ stands for the relative dielectric constant of the smooth waveguide. The permitivity is fixed at the vacuum permeability $\mu_0 = 4\pi \times 10^{-7}\ H/m$ for the walls and interior of the waveguide.

Hollow dielectric waveguides gained interest in the 1970s, when they were considered for laser structures [12, 21, 1, 7, 13, 26, 25]. The waveguide laser requires the use of a multi-moded structure. We are interested in multi–moded waveguides because the normal width of streets is many times the wavelength in the UHF band. We follow the waveguide analysis presented by *Adam and Kneubühl* [1] in the discussion of the smooth lossy hollow waveguide. We consider a slab waveguide of width $2a$ with propagation along the z direction. There is no variation in the y direction so $\frac{\partial}{\partial y} = 0$. The lossy dielectric walls of the waveguide have the relative complex dielectric constant

$$\epsilon = \epsilon' + j\epsilon'' = \epsilon_r - j\frac{\sigma}{\omega\epsilon_0} \qquad (2)$$

where ϵ_r is the permitivity of the walls, σ is their conductivity; ω is the angular frequency, the time dependence is $e^{j\omega t}$ and $\epsilon_0 = 8.85 \times 10^{-12}\ \frac{F}{m}$ is the vacuum dielectric constant. We present a few other definitions: $k = \frac{2\pi}{\lambda}$ is the free space wave number, where λ is the free space wavelength. β and $k_x = u/a$ represent the z and x components of the k vector for propagation inside the waveguide, where u is the normalized k vector in the x direction. In the walls of the waveguide, the propagation constant is $k_2 = \left(\epsilon\mu_0 w^2\right)^{1/2}$ and its x component is $k_a = q/a$ where q is normalized. $Z_0 = \sqrt{\frac{\mu_0}{\epsilon_0}}$ is the vacuum impedance, and $\mathcal{H}$ is an arbitrary amplitude.

The electric field for the TE modes inside the waveguide $|x| <= a$ is given in [1]:

$$E_y = j\frac{k}{k_x} Z_0 \mathcal{H} \left\{ \begin{array}{c} \cos(k_x x) \\ \sin(k_x x) \end{array} \right\} e^{j\omega t - j\beta z} \qquad (3)$$

with similar expressions for the magnetic field of the TM modes. The upper function applies to the symmetric modes and the lower to the antisymmetric modes.

Using the boundary conditions, the characteristic equation can be formulated in terms of u, the propagation constant in the waveguide and R, which represents the properties of the waveguide. An exact solution of the characteristic equations is very difficult. *Burke* [4] gives a graphical solution for the TE case but we follow [1] and discuss an approximate solution. We assume that the imaginary parts of ϵ and u are small compared to their real parts. In order to test the assumption on ϵ we calculate a typical value using the electrical properties of brick: relative electrical permitivity $\epsilon_r = 4.44$ and conductivity $\sigma = 0.01$ S/m [14]. We consider radiation at 1 GHz and get $\epsilon = 4.44 - j0.18$, so the imaginary part is significantly smaller than the real part and the assumption on ϵ holds. The assumption on u relies on observing the solution

obtained elsewhere (for example, in a graphical method).

Under these approximations on u and ϵ, the characteristic values of the real part of u are [1] for the TE modes:

$$u' = \pi(1-\eta)\frac{n}{2}$$

Odd values of n correspond to the symmetrical modes and even values of n correspond to anti-symmetrical modes. The imaginary part of u is small in all cases, as assumed.

The propagation constant in the z direction is determined from $\beta^2 = k^2 - (\frac{u}{a})^2$. By separating real and imaginary parts and neglecting terms of second degree we obtain the approximations for $\beta = \beta' + j\beta''$ [1]:

$$\beta' = \left[\left(\frac{2\pi}{\lambda}\right)^2 - \left(\frac{u'}{a}\right)^2\right]^{1/2} \tag{4}$$

The imaginary part for the TE modes is given by:

$$\beta'' = \frac{\lambda^2}{4a^3(\epsilon'-1)^{1/2}}\left(\frac{n}{2}\right)^2 \quad n = 1, 2, \ldots \tag{5}$$

The number of significant modes N (for a single polarization) can be approximated by $N \approx \frac{2a}{\lambda}$. When both TE and TM modes are considered, the number of significant modes is $2N$.

2.1.1 The Power Carried by the Modes

Next, we calculate the power carried by the different modes, in order to normalize them at a later stage. The Poynting vector is given by

$$S = \frac{1}{2}\text{real}\,(\mathbf{E} \times \mathbf{H}^*) \tag{6}$$

and the power (per unit length in the y direction) is calculated by

$$P = \int_{-a}^{a} S_z dx \tag{7}$$

where we disregard the power propagating inside the walls of the waveguide. We assume here the convention that the mode amplitudes $\mathcal{H}_n$ are normalized so that all the modes carry the same amount of power. We also assume that the modal amplitudes $\mathcal{H}_n$ are real and positive. When we consider later modes with different power levels or with complex amplitudes, we use a multiplicative coefficient for each mode. The power carried by each TE mode is given by

$$P = \frac{k\beta'_m a^3}{2u'^2_m} Z_0 \mathcal{H}_m^2 = \frac{ka^3 Z_0}{2}\frac{\sqrt{\beta'_m}\mathcal{H}_m}{u'_m}\frac{\sqrt{\beta'_n}\mathcal{H}_n}{u'_n} \tag{8}$$

where the last equation in (8) is due to our assumption of equal power carried by all the modes. The power carried by the TM modes can be expressed with a similar formula.

2.1.2 The Orthogonality of the Modes

We refer to two modes as orthogonal if the power carried by their combined fields when they propagate in the waveguide can be expressed as the sum of the powers carried by each mode separately. If P_T is the total power measured in a waveguide and $\{P_n\}_{n=1}^N$ are the powers carried by N propagating modes, then these modes are orthogonal if

$$P_T = \sum_{n=1}^{N} P_n \tag{9}$$

A condition on mode orthogonality can be expressed in terms of the electric fields of the modes. Two modes are orthogonal if

$$I_{nm} = \int_{-a}^{a} \mathbf{E_n} \cdot \mathbf{E_m} dx = 0 \tag{10}$$

where $\cdot$ represents the vector dot product. We now establish the orthogonality of the modes in the smooth waveguide. It is important because these modes are used in section 2.2 as a basis for the representation of other waveforms. Clearly, any TE mode is orthogonal to any TM mode as their respective electric fields are geometrically orthogonal.

The modes of the hollow slab are approximately orthogonal, under the assumptions

$$u'' << u' \tag{11}$$

$$\eta << 1 \tag{12}$$

This can be verified by inserting the field expressions (3) in (10).

2.2 A Rough Waveguide

In order to model realistic surfaces of buildings we must take into account the fact that they are not perfectly smooth. In this section we consider

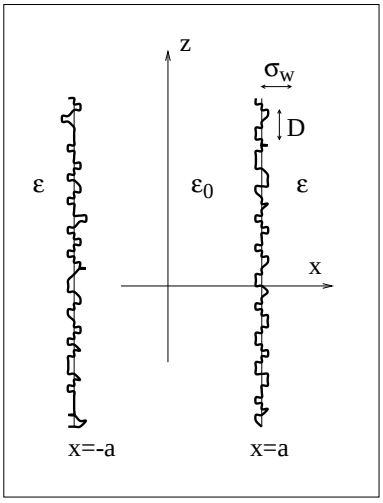

Figure 2: A rough slab waveguide

slab waveguides made of uniform material, but the geometry of the walls is no longer perfectly smooth, as shown in figure 2.

The analysis of multi-moded waveguides and the coupling between the propagating modes started with a series of papers by *Marcuse* [16, 17, 18, 22, 19, 20] and was extended by others [6, 11, 5, 10, 29]. We follow the approach taken by *Marcuse* [16] to analyze the mode coupling caused by the roughness of the waveguide walls. We follow a perturbation analysis of the waveguide, which uses the modes of the smooth waveguide as a basis; the analysis relies on the assumption of small perturbations of the wall geometry.

We maintain the two dimensional model, where there is no variation in the y direction. The wall boundary near $x = a$ is given by the function $x = f(z)$ and the boundary near $x = -a$ is given by $x = h(z)$. We characterize the wall perturbations statistically, using their correlation functions, where we assume that the perturbation on both walls are independent of each other and wide sense stationary, i.e., the statistical propertied do not change along the street. for any point z_0 along the waveguide:

$$\langle [f(z_0) - a]\,[f(z_0 + z) - a] \rangle = \sigma_w^2 e^{-\frac{|z|}{D}} \qquad (13)$$

where σ_w is the rms deviation of the wall from perfect straightness and D is the correlation length. We assume the same statistics for $h(z)$, which defines the deviations of the wall near $x = -a$. The Gaussian correlation assumption may not be accurate, but it captures two important features of every correlation function, namely a correlation length and a variance.

We now examine the deviation of the complex dielectric constant of the waveguide from the smooth waveguide. Near the boundary $x = a$ this deviation is given by

$$\epsilon_r(x,z) - \epsilon_s(x,z) = \Delta\epsilon(x,z) =$$
$$\begin{cases} 0 & \begin{cases} x < a & a < f(z) \\ x < f(z) & f(z) < a \end{cases} \\ 1-\epsilon & a < x < f(z) \quad a < f(z) \\ -(1-\epsilon) & f(z) < x < a \quad f(z) < a \\ 0 & \begin{cases} x > f(z) & f(z) > a \\ x > a & a > f(z) \end{cases} \end{cases}$$

where $\epsilon_r(x,z)$ stands for the relative dielectric constant of the rough waveguide and $\epsilon_s(x,z)$ is defined in (1). The deviation near $x = -a$ is expressed in a similar manner, in terms of $h(z)$.

The fields in the waveguide are the solutions of the wave equation:

$$\frac{\partial^2 E_y}{\partial x^2} + \frac{\partial^2 E_y}{\partial z^2} + (\epsilon_s(x,z) + \Delta\epsilon(x,z))\,\epsilon_0 k^2 E_y = 0$$

The modes of the smooth waveguide are the solutions of

$$\frac{\partial^2 E_y}{\partial x^2} + \frac{\partial^2 E_y}{\partial z^2} + \epsilon_s(x,z)\epsilon_0 k^2 E_y = 0 \qquad (14)$$

We express the fields in the perturbed waveguide in terms of the modal fields of the smooth waveguide:

$$E_y = \sum_{n=1}^{N} C_n(z) E_{yn} \qquad (15)$$

where $C_n(z)$ are complex modal coefficients. The summation in (15) is taken over all the symmetric and antisymmetric TE modes. When we insert this expansion in equation (2.2), we get an equation in terms of the modal coefficients $C_n(z)$:

$$\sum_n \frac{\partial^2 C_n(z)}{\partial z^2} E_{yn} + 2\sum_n (-j\beta_n)\frac{\partial C_n(z)}{\partial z} E_{yn}$$
$$+\Delta\epsilon(x,z)\epsilon_0 k^2 \sum_n C_n(z) E_{yn} = 0 \qquad (16)$$

We multiply this equation by the expression of the field of a specific mode, E_{ym}, and integrate

from $x=-a$ to $x=a$. The orthogonality of the modes of the smooth waveguide is very useful at this stage, because it removes most of the terms in the integral, and we are left with a differential equation for the coefficient of the m$^{\text{th}}$ mode:

$$\frac{\partial^2 C_m}{\partial z^2} - 2j\beta_m \frac{\partial C_m}{\partial z} = F_m(z) \qquad (17)$$

Where $F_m(z)$ is given by:

$$F_m(z) = -\epsilon_0 k^2 \int_{-a}^{a} \Delta\epsilon(x,z) \sum_n C_n(z) E_{yn} E_{ym}^* dx \qquad (18)$$

We now calculate the coupling between the 1$^{\text{st}}$ mode and all the other modes. This result is later extended and we derive the coupling coefficient between any two modes. The 1$^{\text{st}}$ mode is not particularly different from the other modes. We choose to use it for the calculation of the coupling coefficient for the ease of notation.

In order to calculate the coupling coefficients between the 1$^{\text{st}}$ mode and the other modes, we assume that the 1$^{\text{st}}$ mode is excited at $z=0$ and calculate the amplitudes of the other modes at a point z.

$$C_m(0) = \begin{cases} 1 & m=1 \\ 0 & m>1 \end{cases} \qquad (19)$$

We assume that coupling is low, which means that either the point z is close enough to zero or that coupling is so small that second order coupling is negligible. We consider only the coupling of power from the 1$^{\text{st}}$ mode into other modes, and disregard coupling among the higher order modes. We also neglect the coupling from any mode into the 1$^{\text{st}}$ mode.

We solve equation (17):

$$\begin{aligned} C_m(z) &= A_m + B_m e^{2j\beta_m z} \qquad (20) \\ &\quad + \frac{1}{2j\beta_m} \int_0^z \left[e^{2j\beta_m (z-\zeta)} - 1 \right] F_m(\zeta) d\zeta \end{aligned}$$

The coupling coefficient (20) contains forward traveling (toward $+z$) and backward traveling waves:

$$C_m = C_m^{(+)} + C_m^{(-)} \qquad (21)$$

where the forward traveling part is

$$C_m^{(+)}(z) = A_m - \frac{1}{2j\beta_m} \int_0^z F_m(\zeta) d\zeta \qquad (22)$$

Using the low coupling assumption (explained below (19)), we disregard the backward traveling waves and use the approximation $C_m(z) \approx C_m^{(+)}(z)$. After applying the initial conditions (19), the coupling coefficients are then given by

$$C_m(z) = -\frac{1}{2j\beta_m} \int_0^z F_m(\zeta) d\zeta \quad m>1 \qquad (23)$$

Using the low coupling assumption we calculate $F_m(z)$ from (18):

$$\begin{aligned} F_m(z) &\approx -\frac{\beta_m k^2}{2\omega\mu_0 P}(1-\epsilon) \\ &\quad \times \left[(f(z)-a)\, E_1(a,z) E_m^*(a,z) \right. \\ &\quad \left. - (h(z)+a)\, E_1(-a,z) E_m^*(-a,z) \right] \end{aligned} \qquad (24)$$

where P is the power carried by each mode. The difference in the power levels of the modes are expressed with the modal coefficients C_n.

For the TE modes, we use the field expressions from (3):

$$\begin{aligned} E_1(a,z) E_m^*(a,z) &= E_1(-a,z) E_m^*(-a,z) \\ &\approx \frac{(kd)^2}{u_1' u_m'} Z_0^2 \mathcal{H}_1 \mathcal{H}_m T_1(u_1') T_m(u_m') \\ &\quad \times e^{j(\beta_1 - \beta_m) z} \end{aligned} \qquad (25)$$

where

$$T_n(v) = \begin{cases} \cos(v) & n \text{ odd}, \quad \text{TE symmetric} \\ \sin(v) & n \text{ even}, \quad \text{TE antisymmetric} \end{cases} \qquad (26)$$

Rearranging $F_m(z)$ we get

$$\begin{aligned} F_m(z) &\approx (\epsilon - 1) \frac{k^2 \beta_m}{a} \frac{T_1(u_1')}{\sqrt{\beta_1'}} \frac{T_m(u_m')}{\sqrt{\beta_m'}} \\ &\quad \times [f(z) - a - h(z) - a] \\ &\quad \times e^{j(\beta_1 - \beta_m) z} \end{aligned} \qquad (27)$$

Now we calculate the integral in (22):

$$\begin{aligned} \int_0^z F_m(\zeta) d\zeta &\approx (\epsilon - 1) \frac{k^2 \beta_m z}{a} \frac{T_1(u_1')}{\sqrt{\beta_1'}} \frac{T_m(u_m')}{\sqrt{\beta_m'}} \\ &\quad \times (\phi_m^* - \psi_m^*) \end{aligned} \qquad (28)$$

where

$$\phi_m = \frac{1}{z} \int_0^z (f(\zeta) - a) e^{-j(\beta_1 - \beta_m)\zeta} d\zeta \qquad (29)$$

$$\psi_m = \frac{1}{z} \int_0^z (h(\zeta) + a) e^{-j(\beta_1 - \beta_m)\zeta} d\zeta \qquad (30)$$

ϕ_m and ψ_m are the Fourier coefficients of the functions $f(z) - a$ and $h(z) + a$ calculated at the spatial frequency $\beta_1 - \beta_m$, the difference of frequencies between the two coupled modes E_1 and E_m. The coupling between the two modes is related to a particular Fourier component of the geometry of the walls, which corresponds to the spatial frequency difference between the modes. This is a well known result of electromagnetic scattering theory [28, 24].

We calculate the modal coefficients by using (28) in (23):

$$C_m = -(\epsilon - 1)\frac{k^2 z}{2ja}\frac{T_1(u_1')}{\sqrt{\beta_1'}}\frac{T_m(u_m')}{\sqrt{\beta_m'}}(\phi_m^* - \psi_m^*) \quad m > 1 \tag{31}$$

2.2.1 The Coupled Power Equations

The coupling coefficients of the modes contain amplitude and phase information, but the quantity that interests us most is the power carried by the different modes. The coupling coefficients C_n contain too much information for our needs. We are interested in the power exchange among the modes, which is best expressed in terms of power equations. We now proceed to derive the coupled power equations of the modes of the rough waveguide, following *Marcuse* [18]. The derivation is based on the above calculation of the complex coupling coefficients of the waveguide modes.

The coupling coefficients of the modes affect the mode amplitudes through the wave equation

$$\frac{\partial A_m}{\partial z} = \sum_{n=1}^{N} c_{mn} A_n \tag{32}$$

where A_n represent the complex mode amplitudes (phasor) and c_{mn} is the coupling coefficient from the n$^{\text{th}}$ mode to the m$^{\text{th}}$. c_{nn} represents the propagation constants of the n$^{\text{th}}$ mode, so $c_{nn} = -j\beta_n$. We represent the harmonic z dependence of the modes explicitly:

$$A_n(x,z) = C_n(z)B_n(x)e^{-j\beta_n z} \tag{33}$$

where $B_n(x)$ contains the x dependence of the n$^{\text{th}}$ mode. The coupled equations in terms of the new notation are:

$$\frac{\partial C_m}{\partial z}B_m(x) = \sum_{\substack{n=1 \\ n\neq m}}^{N} c_{mn}C_n B_n(x)e^{j(\beta_m - \beta_n)z} \tag{34}$$

In order to calculate the coupling coefficients c_{mn}, we solve (34), with the initial conditions defined in (19): at $z = 0$ only the 1$^{\text{st}}$ mode is excited. Using a first order perturbation solution we get:

$$C_m(z) \approx \begin{cases} 1 & m = 1 \\ c_{m1} z e^{j(\beta_m - \beta_1)z} & m > 1 \end{cases} \tag{35}$$

A comparison of (35) with (31) gives the coupling coefficient from the 1$^{\text{st}}$ mode to the m$^{\text{th}}$:

$$c_{m1} = -(\epsilon - 1)\frac{k^2}{2ja}\frac{T_1(u_1')}{\sqrt{\beta_1'}}\frac{T_m(u_m')}{\sqrt{\beta_m'}} \times [f(z) - a - h(z) - a] \tag{36}$$

We extend this result and assume that the coupling from the n$^{\text{th}}$ mode to the m$^{\text{th}}$ is described by:

$$c_{mn} = -(\epsilon - 1)\frac{k^2}{2ja}\frac{T_n(u_n')}{\sqrt{\beta_n'}}\frac{T_m(u_m')}{\sqrt{\beta_m'}} \times [f(z) - a - h(z) - a] \tag{37}$$

The coupling coefficients are reciprocal, i.e.

$$c_{mn} = -c_{nm}^* \tag{38}$$

The reciprocity can be shown by considering the preservation of power of the coupling process. For details see *Marcuse* [18].

A further extension of the calculation of the coupling coefficients applies the result to the TM modes. We present a new indexing method which is used in the remainder of the paper. The TE modes are numbered $1, \ldots, N$ and the TM modes are numbered $N+1, \ldots, 2N$. When using the propagation constants u_n and β_n for $n > N$, we apply the appropriate formulas with $n - N$.

The waveguide model we presented in this section does not introduce coupling between TE and TM modes. However, a realistic model which allows for variations in the y direction does introduce such coupling. We include TE–TM coupling in our model and assume that the coupling

coefficients are given by (37) with:

$$T_n(v) = \begin{cases} \cos(v) & \begin{cases} 1 \le n \le N,\ n \text{ odd}, \\ \text{TE symmetric} \end{cases} \\ \sin(v) & \begin{cases} 1 \le n \le N,\ n \text{ even}, \\ \text{TE antisymmetric} \end{cases} \\ \sin(v) & \begin{cases} N+1 \le n \le 2N \\ (n-N) \text{ even}, \\ \text{TM symmetric} \end{cases} \\ \cos(v) & \begin{cases} N+1 \le n \le 2N \\ (n-N) \text{ odd}, \\ \text{TM antisymmetric} \end{cases} \end{cases}$$

The coupled wave equations (32) are translated into a system of coupled power equations using *Marcuse*'s theory [18]. The average power carried by the n$^{\text{th}}$ mode is $P_n = \left\langle |A_n|^2 \right\rangle = \left\langle |C_n|^2 \right\rangle$, where the brackets $\langle \cdot \rangle$ indicate an ensemble average over many waveguides with (statistically) similar wall perturbations. An important assumption in the development of this theory is that the coupling coefficients are of the form

$$c_{mn} = K_{mn}\gamma(z) \tag{39}$$

where $\gamma(z)$ has the following correlation properties:

$$\langle \gamma(z)\gamma(z-z_0) \rangle = \sigma_\gamma^2 e^{-\left(\frac{|z_0|}{D_\gamma}\right)^2} \tag{40}$$

The coupled power equations are [18]:

$$\begin{aligned} \frac{dP_m}{dz} &= -\alpha_m P_m + \sqrt{\pi}\sigma_\gamma^2 D_\gamma \\ &\quad \times \sum_{n=1}^{2N} |K_{mn}|^2 \, e^{-\left[\frac{D_\gamma}{2}(\beta_m - \beta_n)\right]^2} \\ &\quad \times (P_n - P_m) \end{aligned} \tag{41}$$

where α_m are arbitrary modal loss factors. These factors do not emerge from the theory; they are introduced in order to account for physical effects. In the case of the street waveguide we use the coupling coefficients calculated in (37), and realize that

$$K_{mn} = -(\epsilon - 1)\frac{k^2}{2ja}\frac{T_n(u_n')}{\sqrt{\beta_n'}}\frac{T_m(u_m')}{\sqrt{\beta_m'}} \tag{42}$$

and $\gamma(z) = f(z) - h(z) - 2a$. Using (13) we calculate the correlation of $\gamma(z)$:

$$\sigma_\gamma = \sqrt{2}\sigma_w \tag{43}$$

$$D_\gamma = D \tag{44}$$

A natural choice for the loss factors α_m is the modal loss factors β_m'' calculated in (5). When we compare the theoretical predictions of our model to actual measurements (section 3) we discover that realistic power loss factors are higher than those warranted by the simplified waveguide model.

The coupled power equations (41) can be expressed as a simple matrix equation, where the unknown is a vector containing the power level of each mode:

$$\overline{P} = \begin{pmatrix} P_1 \\ \vdots \\ P_{2N} \end{pmatrix} \tag{45}$$

and the coupled power equation takes the form:

$$\frac{\partial \overline{P}}{\partial z} = \Gamma \overline{P} \tag{46}$$

Γ is an $2N \times 2N$ matrix which holds all the power coupling coefficients. The mn$^{\text{th}}$ location holds

$$\Gamma_{mn} = \sqrt{\pi} 2\sigma_w^2 D |K_{mn}|^2 e^{-\left[\frac{D}{2}(\beta_m - \beta_n)\right]^2} \tag{47}$$

and the diagonal elements hold the sum of the coupling coefficients and the loss of each mode

$$\begin{aligned} \Gamma_{mm} &= -\alpha_m - \sqrt{\pi} 2\sigma_w^2 D \\ &\quad \sum_{\substack{n=1 \\ n \neq m}}^{N} |K_{mn}|^2 e^{-\left[\frac{D}{2}(\beta_m - \beta_n)\right]^2} \end{aligned} \tag{48}$$

2.2.2 Solution of the Coupled Power Equations

The coupled power equation (46) is easily solved in terms of the eigenvalues and eigenvectors of the coupling matrix Γ. When we used realistic street parameters in simulations, all the power in steady state tended to concentrate in the lower order TE mode.

We also looked at the dynamic behavior of the power measured at small distances from a source. We model the source as a distribution of power among the waveguide modes, and then solve (46) numerically. The results we present in section 3 are the total power along the waveguide predicted using this method.

2.3 A Street Corner Model

This section describes the model of street corners, where power flows along one street (the 'main' street) into another ('side') street. We are interested in the behavior of power levels along the side street. We present here an intuitive explanation of the mode coupling mechanism. For a more thorough analysis see [3]. In order to look at this coupling mechanism in some detail, we consider the plane wave decomposition of the modes.

Each mode can be decomposed into a pair of plane waves propagating at equally oblique angles with the z direction. The lower order modes are decomposed into plane waves that propagate in an almost parallel direction to the z axis. High order modes travel in directions increasingly oblique to the z axis. When considering a perpendicular street corner, the low order modes in the main street couple into high order modes in the side street and vice versa.

We assume steady state distribution of power of the modes in the main street, where most of the power is contained in the low order modes. As a consequence, the power coupled into the side street is mostly contained in the high order modes. The power leaking into the side street is re-distributed among the modes as it propagates along the street.

The expected effect in the side street is a significant decrease of power level as the receiver moves away from the junction. At a certain distance, where the modal distribution of power reaches its steady state, the rate of decrease of power loss along the street resumes its steady state rate.

3 Comparison to Measurements

We compare our theoretical predictions of the rate of power loss along a side street with actual measurements. The measurements we show in this section were obtained from two sources: Measurements in the 900 MHz band taken by Dr. E. Damosso and Dr. L. Stola of CSELT, Italy in Turin, Italy in 1992 and measurements at 910 MHz taken by Dr. J. H. Whitteker in Ottawa, Ontario, Canada in 1986 [30][1]. The measurements we show were taken in side streets, with a mobile receiver moving away from a junction of the side street and another street that contained a transmitter. The measurements were filtered over 2 m sections along the street; the Turin measurements were averaged over samples taken at 5 cm intervals and the Ottawa measurements were median filtered over non-uniform sampling distances, in the range of 1–2 m.

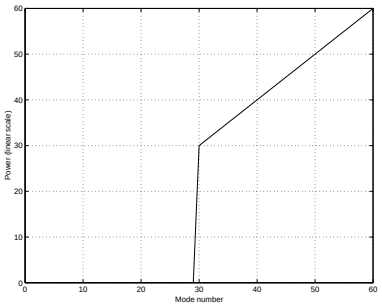

Figure 3: 'High Order' initial power distribution for the TE and TM modes, for the case of 120 modes. The vertical axis is linear, in relative units.

We used the approximate widths of the streets in the calculations, but other parameters were adjusted to give the best match between measurement and theory. It is difficult to measure these parameters since they represent a simplified model of a true street. However, we used values that appear to be within realistic ranges. The geometric perturbation variance was set between 20 cm and 1 m and the geometric correlation length was between 10–40 m, which corresponds to the dimensions of external features of buildings.

The distribution of power among the modes at the side street very close to the junction provides an initial condition for our simulation. We used the following initial conditions in the simulations, as indicated in table 1.

- The 'High Order' (H.O.) initial power distribution has no power in the lower half of the modes and linearly increasing power at the higher half, as seen in figure 3.
- The 'Uniform' (U.) initial power distribution assigns a constant power level to all the

[1] See Acknowledgment

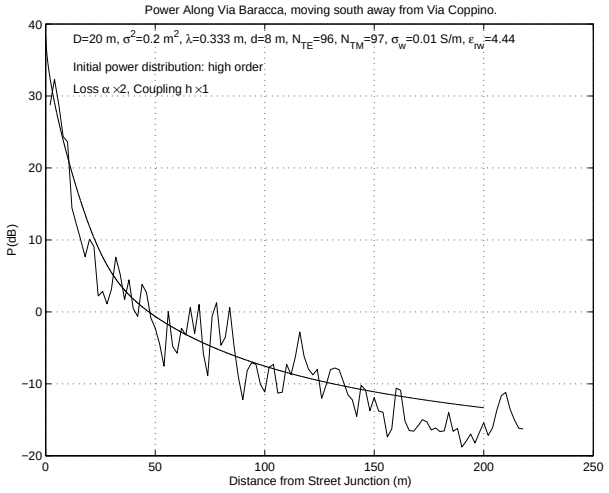

Figure 4: Measurements taken in Via Baracca, Turin, Italy, moving north away from Via Coppino (that contained the transmitter). See simulation parameters is table 1.

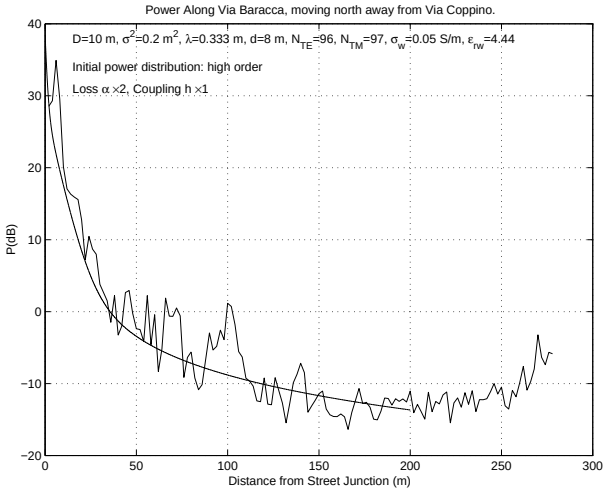

Figure 5: Measurements taken in Via Baracca, Turin, Italy, moving south away from Via Coppino (that contained the transmitter). See simulation parameters is table 1.

propagating modes

Initial power distributions that assign power to the high order modes are reasonable when considering the coupling of power from the main street, where steady state distribution was attained (which concentrated power in the low order modes), into the side street (see section 2.3).

We multiplied the loss factors β'' (from (5)) by factors varying between 2 to and 3, to account for the losses in the streets. The multiplication factors are indicated in table 1. This increase of loss was needed to fit the calculations to the measurements. In one case (figure 6) we also multiplied the coupling coefficients (c_{mn}, $m \neq n$) by 2.

Figures 4–8 show comparisons between the theory and measurements. The measurements are shown with a broken line and the theoretical prediction with a smooth line. The parameter values used in the simulations are summarized in table 1. In some of the figures (for example, figure 5) an increase in the measured power level is evident near the rightmost part of the graph, at large distances from the intersection. This behavior is caused by the proximity of a second street corner that couples power into the street in the backward (-z) direction. This effect was not taken into account in the theoretical calculation.

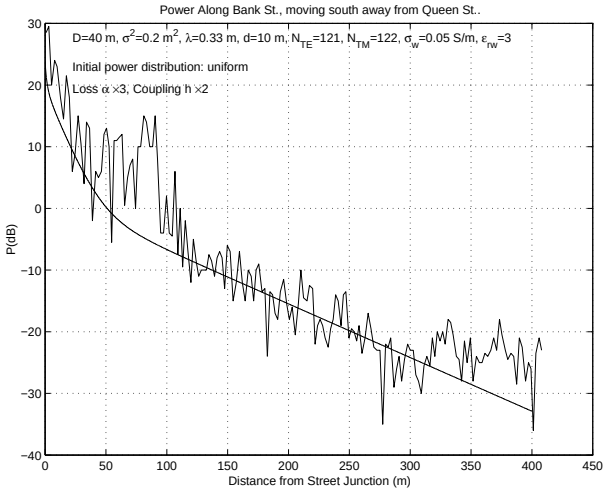

Figure 6: Measurements taken in Bank St., Ottawa, Canada, moving south away from Queen St. (that contained the transmitter). See simulation parameters is table 1.

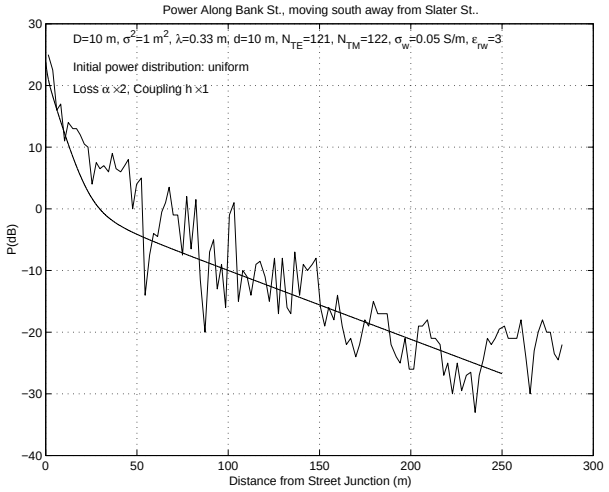

Figure 7: Measurements taken in Bank St., Ottawa, Canada, moving south away from Slate St. (that contained the transmitter). See simulation parameters is table 1.

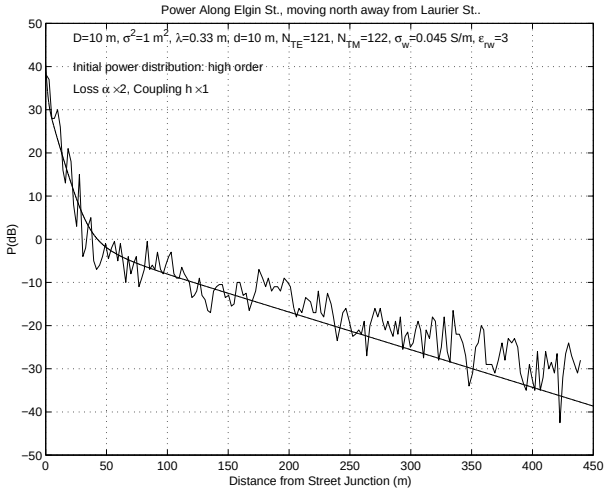

Figure 8: Measurements taken in Elgin St., Ottawa, Canada, moving north away from Laurier St. (that contained the transmitter). See simulation parameters is table 1.

Figure Number	4	5	6	7	8
Frequency (MHz)	900	900	910	910	910
Correlation Length D (m)	20	10	40	10	10
Perturb. Variance σ_w^2 (m^2)	0.2	0.2	0.2	1	1
Street Width $2a$ (m)	16	16	20	20	20
Number of Modes (TE and TM)	192	192	242	242	242
Wall Conduct. σ (S/m)	0.01	0.05	0.05	0.05	0.045
Wall Permitivity ϵ_r (relative)	4.44	4.44	3	3	3
Initial Power Distrib.	H.O.	H.O.	U.	U.	H.O.
Loss Multip. Factor	2	2	3	2	2
Coupling Multip. Factor	1	1	2	1	1

Table 1: Simulation parameters. The initial power distribution is one of 'High Order' (H.O.) or 'Uniform' (U.).

4 Conclusion

We presented a new approach to propagation predictions in the UHF band in urban environments. Streets are modeled as hollow waveguides bound by very large lossy plates on both sides. We included the effects of the roughness of the external walls of the buildings by introducing mode coupling.

Using a perturbation model for the mode coupling induced by the walls, the coupled power equations were developed, which relate the power levels of the modes as they propagate away from a source.

The theory was used to predict the decrease of the power recorded by a mobile receiver as it moves away from a junction with line of sight to a transmitter into a street with no such line of sight. Comparisons of the theoretical predictions and actual measurements show good agreement.

Acknowledgments

The authors thank Dr. James H. Whitteker of Northwood Technologies Inc., Ontario, Canada and Dr. Eraldo Damosso and Dr. Loris Stola of CSELT, Italy for providing us with their measurement data and permitting us to use these data.

References

[1] B. Adam and F. Kneubühl. Transversely excited 337 μm HCN waveguide laser. *Appl. Phys.*, 8(4):281–291, December 1975.

[2] M. Barbiroli, V. Degli Eposti, and P. Grazioso. Extraction of a simplified model for street corner loss in microcells from ray-tracing simulation. *Wireless Personal Communications*, 12:225–237, 2000.

[3] N. Blaunstein. *Radio Propagation in Cellular Networks*. Artech House, 2000.

[4] J. J. Burke. Propagation constants of resonant waves on homogeneous, isotropic slab waveguides. *Applied Optics*, 9(11):2444–2452, November 1970.

[5] G. Cancillieri and P. Fantini. Mode coupling effects in optical fibres: perturbative solution of the time-dependent power flow equation. *Optical and Quantum Electronics*, 15:119–136, 1983.

[6] B. Crosignani, C. H. Papas, and P. Di Porto. Theory of time-dependent propagation in mulitmode lightguides. *J. Opt. Soc. Am.*, 67(10):1300–1307, October 1977.

[7] J. J. Degnan. The waveguide laser: A review. *Appl. Phys.*, 11(1):1–33, September 1976.

[8] A. G. Emslie, R. L. Lagace, and P. F. Strong. Theory of the propagatio nof UHF radio waves in coal mine tunnels. *IEEE Trans. on Ant. and Prop.*, AP-23(2):192–205, March 1975.

[9] B. Erceg, S. Ghassemzadeh, M. Taylor, D. Li, and D. L. Schilling. urban/suburban out-of-sight propagation modeling. *IEEE Communications Magazine*, pages 56–61, June 1992.

[10] D. G. Hall. In-phase scattering in planar optical waveguides: refractive-index fluctuations and surface roughness. *J. Opt. Soc. Am. A*, 2(5):747–752, May 1985.

[11] W. E. Kohler. Propagation in a randomly perturbed mulitmode matched waveguide. *Wave Motion*, 4:243–263, 1982.

[12] H. Krammer. Field configurations and propagation constants of modes in hollow rectangular dielectric waveguides. *IEEE J. of Quantum Electronics*, pages 505–507, August 1976.

[13] K. D. Laakmann and W. H. Steier. Waveguides: characteristic modes of hollow rectangular dielectric waveguides. *Applied Optics*, 15(5):1334–1340, May 1976.

[14] O. Landron, M. J. Feuerstein, and T. S. Rappaport. A comparison of theoretical and empirical reflection coefficients for typical exterior wall surfaces in a mobile radio environment. *IEEE Trans. on Ant. and Prop.*, 44(3):341–351, March 1996. Table I.

[15] S. F. Mahmoud and J. R. Wait. Geometrical optical approach for electromagnetic

wave propagation in rectangular mine tunnels. *Radio Science*, 9(12):1147–1158, December 1974.

[16] D. Marcuse. Mode conversion caused by surface imperfactions of a dielectric slab waveguide. *The Bell Sys. Tech. J.*, pages 3187–3215, December 1969.

[17] D. Marcuse. Radiation losses of dielectric waveguides in terms of the power spectrum of the wall distortion function. *The Bell Sys. Tech. J.*, pages 3233–3242, December 1969.

[18] D. Marcuse. Derivation of coupled power equations. *The Bell Sys. Tech. J.*, 51(1):229–237, January 1972.

[19] D. Marcuse. Fluctuatios of the power of coupled modes. *The Bell Sys. Tech. J.*, 51(8):1793–1800, October 1972.

[20] D. Marcuse. Higher-order loss processes and the loss penalty of multimode operation. *The Bell Sys. Tech. J.*, 51(8):1819–1836, October 1972.

[21] D. Marcuse. Hollow dielectric waveguide for distributed feedback lasers. *IEEE J. of Quantum Electronics*, QE-8(7):661–669, July 1972.

[22] D. Marcuse. Power distributions and radiation losses in multimode dielectric slab waveguides. *The Bell Sys. Tech. J.*, 51(2):429–454, February 1972.

[23] D. Marcuse. *Theory of Dielectric Optical Waveguides*. Academic Press, second edition, 1991.

[24] S. E. Miller. coupled wave theory and waveguide applications. *The Bell System Technical J.*, pages 661–719, May 1954.

[25] M. Nomoto, S. Abe, and M. Miyagi. Graphical representation of mode selectivity in hollow waveguides with and without inner dielectric layer: slab waveguide model. *Optics Communications*, 108:243–246, June 1994.

[26] D. Pasquet. Accurate graphic resolution of the characteristic equations of a hollow dielectric slab wavbeguide. *International J. of Infrared and Millimeter Waves*, 2(3):453–463, 1981.

[27] Theodore S. Rappaport. *Wireless Communications Principles and Practices*. Prentice Hall PTR, 1996. Table 3.1.

[28] S. O. Rice. Reflection of electromagnetic waves from slightly rough surfaces. In M. Kline, editor, *The Theory of Electromagnetic Waves*, pages 315–378. Dover Publications, 1965. Reprint of a 1951 publication of Interscience Publishers.

[29] D. Swierk and A. Heimrath. Random multimode optical media: I. mode coupling process in slab waveguide with stochastic wall perturbations. *J. of Modern Optics*, 39(4):681–688, 1992.

[30] James H. Whitteker. Measurements of path loss at 910 MHz for proposed microcell urban mobile systems. *IEEE Trans. on Vehicular Technology*, 37(3):125–129, August 1988.